Applied Physics Letters

High performance non-fullerene organic photovoltaics under implant light illumination region

Cite as: Appl. Phys. Lett. **122**, 143906 (2023); https://doi.org/10.1063/5.0144861
Submitted: 01 February 2023 • Accepted: 21 March 2023 • Published Online: 07 April 2023
Published open access through an agreement with JISC Collections

Ram Datt, Harrison Ka Hin Lee, Michael Spence, et al.

Applied Physics Letters ARTICLE scitation.org/journal/apl

High performance non-fullerene organic photovoltaics under implant light illumination region

Cite as: Appl. Phys. Lett. **122**, 143906 (2023); doi: 10.1063/5.0144861
Submitted: 1 February 2023 · Accepted: 21 March 2023 ·
Published Online: 7 April 2023

View Online Export Citation CrossMark

Ram Datt, Harrison Ka Hin Lee,[a] Michael Spence, Matthew Carnie, and Wing Chung Tsoi[a]

AFFILIATIONS

SPECIFIC, Faculty of Science and Engineering, Swansea University, Bay Campus, Fabian Way, Swansea SA1 8EN, United Kingdom

[a]Authors to whom correspondence should be addressed: k.h.lee@swansea.ac.uk and w.c.tsoi@swansea.ac.uk

ABSTRACT

Implantable biomedical electronics, such as pacemakers, drug pumps, cochlear implants, cardioverter-defibrillators, and neurological stimulators, help humans to overcome various diseases. Currently, the power supply for these devices relies on small-size batteries, and replacement of the battery is required after running for a period of time. Recharging the battery could be a way to prolong the replacement cycle. Organic photovoltaics (OPVs) are a class of emerging photovoltaics, which are now becoming more practical with recently developed device and material engineering. The absorption of OPVs using a non-fullerene acceptor (NFA) could be extended to the near-infrared (NIR) region to cover the transmission window of human skin between 650 and 1000 nm. Motivated by this, we conducted a study of NFA-based OPVs under light irradiation of wavelengths of 650–1000 nm for implants. The devices using donor (PTB7-Th) and NFA (IEICO-4F) as the active material have strong absorption in the NIR region and obtained a promising power conversion efficiency (PCE) of 14.3% under the implant light illumination, compared to 8.11% when using a benchmark fullerene derivative-based acceptor ($PC_{71}BM$). Importantly, the PCE and power density of the NFA-based OPVs are significantly higher than the previously reported fullerene-based OPVs devices. This study shows that NFA-based OPVs have high potential for future applications in powering implants, e.g., through charging batteries.

Biomedical electronic implants are devices placed inside the body. Common applications include delivering medication, supporting organs and tissues, monitoring body functions, and diagnosing diseases. The power requirement of implant devices can be very low, such as 10–30 μW for a pacemaker, 10–100 μW for a cardiac defibrillator, and 200 μW for artificial urinary sphincters.[1–3] Implant technologies with targeted medical device applications have remarkable ability to make human life better in the near future. However, the power source requirement for operating implantable devices can be a major challenge. Various power sources have been suggested, such as piezoelectric generators, radio frequency harvesters, biofuel cells, thermal electric generators, and batteries.[4,5] Nevertheless, the use of batteries is dominant. However, the replacement of batteries requires a surgical procedure, which is a costly and risky (e.g., infections and bleeding) practice. Moreover, implant devices with high power consumption require regular charging of the battery.[6]

Photovoltaic (PV) technology can be an effective method to charge the batteries inside the human body. Human tissues absorb some of the incident light, which can restrict the penetration depth of visible light down to less than 2 mm. However, the attenuation of the tissue is lower for certain wavelength ranges. For example, light can penetrate up to 4 mm and 1 cm with wavelengths near 700–1000 and 1000–1400 nm, respectively.[3,7] The extended penetration depth of near-infrared (NIR) light can be used to operate PV cells implanted under the skin. Song *et al.*[8] investigated arrays of double junction (GaInP/GaAs) microcells as a candidate for implant photovoltaic (IPV) devices, testing them under human hand dorsum skin (thickness ∼ 0.68 mm) isolated from a cadaver. The PCE of the IPV device measured under 1 sun air mass (AM) 1.5G was 21.5%, and it decreased to 4.3% after covering with skin under similar irradiation. The main parameter, which was impacted due to the reduction in the incident light intensity, was the short circuit current density (J_{sc}), which decreased from 5.63 to 1.17 mA/cm^2. Open circuit voltage (V_{oc}) and fill factor (FF) values changed from 4.6 to 4.5 V and 0.83 to 0.84, respectively. In another study, Song *et al.*[9] used two live hairless mice for *in vivo* study and used double-junction GaInP/GaAs flexible solar

cell arrays as an IPV device. The IPV was inserted in the back side of both mice having skin thicknesses of 675 and 539 μm, respectively. The IPV was measured under 1 sun AM 1.5G. The power conversion efficiency (PCE) decreased from 21.7% (without skin) to 10% (under the skin), and J_{sc} was the main reduced parameter. A silicon solar module is also investigated under the pig skin flags as an IPV.[10] It delivered an output power of 4941 μW/cm^2 under real sun light. Traditional inorganic PV devices use rigid PV materials, and the fabrication processes are costly (much more costly when trying to make it flexible) and may not be biocompatible.[11–13] Dye-sensitized solar cells (DSSCs) have also been studied for biomedical devices and can produce an output power density of 138.75 μW/cm^2 (underneath 1 mm thick chicken skin) under 980 nm laser illumination.[14,15]

Recently, organic photovoltaics (OPVs) delivered PCE up to 20% and have emerged as a potential PV technology for various applications, including building-integrated PVs, indoor, aerospace, and agrivoltaics.[16–21] In addition, due to their biocompatibility and very high flexibility, OPVs have also been suggested to power biomedical implants.[22–24] Furthermore, the bandgap of organic semiconductors can be easily tuned to optimize light absorption at the NIR region, an operational window for IPV devices.[4,25,26] OPVs have also been suggested for bioelectronic devices. Hsiao *et al.*[27] studied the β-carotene/PTCDI-C8 and P3HT: PCBM OPVs under illumination of the NIR region for bioelectronic interface devices. Wu *et al.*[28] studied a P3HT: PCBM OPV as an electrical source for biological nanodevices. When illuminated at 980 nm (16 mW), it delivered a power output of 17.5 μW/cm^2 with a PCE of 0.0124%.

OPVs refer to PV devices that use carbon-based semiconductors as light-absorbing materials.[29,30] In OPVs, a few years ago, fullerene derivative molecules were used almost ubiquitously as electron acceptors. However, due to their inherent limitations, such as weak light absorption, morphological instability, limited adjustability of energy gap, and poor solubility, they have been replaced with polymers and small molecule-based acceptors, which are known as non-fullerene acceptors (NFAs).[31–34] The high bandgap tunability, improved solubility, and better morphology with electron donors have made NFA promising for OPVs. The potential of enhanced absorption in the NIR region using NFA materials[35,36] could make NFA more suitable for potential implant applications than fullerene derivatives, which has shown very low PCE at NIR. This motivates us to investigate the OPV device based on PTB7-Th IEICO-4F system and compared it with the PTB7-Th: $PC_{71}BM$ system-based device under light illumination (650–1000 nm) for implants for the first time. This work demonstrates the high performance of NFA-based OPVs (compared with fullerene derivative acceptors-based OPVs) for potential implant applications. Our finding is expected to spark further research interest in deeper investigation on the potential of NFA-based OPVs to power implant, e.g., through recharging batteries.

The PTB7-Th and IEICO-4F materials were purchased from 1-material, Canada. $PC_{71}BM$ was purchased from Lumtec, Taiwan. Molybdenum trioxide (MoO_3) and silver (Ag) were purchased from STREM Chemicals and Kurt J. Lesker, respectively. The chlorobenzene, 1,8-diiodooctane (DIO), and 1-chloronaphthalene (CN) solvents were procured from Sigma-Aldrich. All materials were used without purification. Indium tin oxide (ITO) coated glass substrates were purchased from Lumtec, Taiwan. Inverted OPV device structures [ITO/zinc oxide (ZnO)/active layer/MoO_3/Ag, Fig. S1(a)] were fabricated for both PTB7-Th: $PC_{71}BM$ and PTB7-Th: IEICO-4F systems. The energy levels of each material are also shown in Fig. S1(b). For the fabrication process, ITO substrates were cleaned by first sonicated in a soap solution, before rinsed in de-ionized water, then sonicated in acetone, and finally sonicated in isopropanol. The ITO substrates were then plasma cleaned for 2.30 min. The 35 nm thick ZnO layer was formed by spin coating the zinc acetate dehydrate precursor at 4000 rpm for 40 s and then annealed at 150 °C for 10 min. The active layers were prepared using the donor: an acceptor ratio of 1: 1.5 for both PTB7-Th: $PC_{71}BM$ and PTB7-Th: IEICO-4F, dissolved in chlorobenzene with a concentration of 25 mg/ml in both cases. 3% DIO and 4% CN were used as additives with PTB7-Th: $PC_{71}BM$ and PTB7-Th: IEICO-4F systems, respectively. 10 nm MoO_3 and subsequently 100 nm Ag were coated on the active layers using a thermal evaporator operated under a 4×10^{-6} mbar vacuum. The device pixel areas were 0.15 cm^2. The devices were then encapsulated inside a glovebox (filled with dry nitrogen) using glass slides and epoxy.

The photovoltaic characteristics were measured by the LED-based 1 Sun AM1.5 G solar simulator. A Keithley 2400 source meter was used. The 1 sun AM 1.5G irradiation was calibrated by using standard silicon solar cells. Two approaches were involved for measuring the devices for an implant. First, short-pass (1000 nm) and long-pass (650 nm) optical filters were used to obtain illumination at the 650–1000 nm wavelength region. The corresponding measurements were denoted as F650–1000 nm. In the second approach, the emission spectrum of a solar simulator was tuned to the 669–944 nm region (Fig. S2), a close proximity to the 650–1000 nm region. A Thorlabs power meter (Model PM100D) was used to measure the incident light intensity for the selected wavelength regions. Light intensity values of 40.8 and 35.7 mW/cm^2 were estimated for the F650–1000, and 669–944 nm wavelength regions, respectively. Two types of PCE were calculated: one used the light intensity of 1 sun AM 1.5G as the input light intensity [denoted as PCE (A)] while the other one used the light intensity at the ≈650–1000 nm region as the input value [denoted as PCE (B)]. The PCE (B) is a more useful metric to evaluate potential implant applications. The external quantum efficiency (EQE) was measured using a QE X10 system (PV measurement).

Figure 1(a) illustrates the concept of OPV devices underneath human skin to power implant devices. The actual location of the OPV will depend on the specific implant applications. Figure 1(b) shows the normalized ultraviolet-visible (UV-Vis) absorption spectra of the PTB7-Th film, the IEICO-4F film, and the $PC_{71}BM$ solution. Importantly, it shows that while $PC_{71}BM$ has very small portion of absorbance in the 650–1000 nm region, IEICO-4F NFA has dominant absorbance in this region (which could be more promising for potential implant applications). Indeed, this is the reason that we selected IEICO-4F to fabricate the OPV devices for the following study. Figure 1(c) shows the chemical structures of PTB7-Th, IEICO-4F, and $PC_{71}BM$.

The OPV device was first measured under 1 sun AM 1.5G illumination. The current density–voltage (J–V) graph and photovoltaic parameters are shown in Fig. 2 and Table I, respectively. The PTB7-Th: $PC_{71}BM$ device has the V_{oc}, J_{sc}, FF, and PCE (A) of 0.80 V, 16.21 mA/cm^2, 0.66, and 8.54%, respectively. The PTB7-Th: IEICO-4F devices has the V_{oc}, J_{sc}, FF, and PCE (A) of 0.70 V, 21.91 mA/cm^2, 0.60, and 9.35%, respectively. Figures 2(a) and 2(b) also show the J–V characteristics under F650–1000 nm and 669–945 nm illumination of the PTB7-Th: $PC_{71}BM$ and PTB7-Th: IEICO-4F devices, respectively.

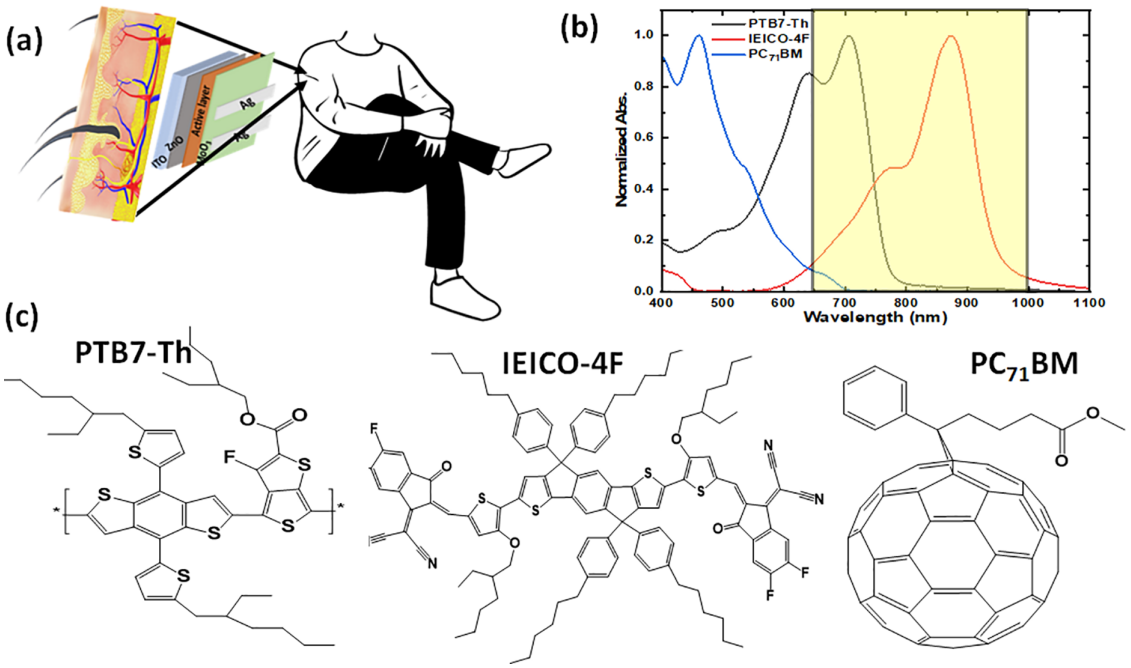

FIG. 1. (a) Concept of OPV implantation under human skin. (b) Normalized UV-Vis absorption spectra of $PC_{71}BM$ (solution), PTB7-Th and IEICO-4F pristine films (the 650–1000 nm wavelength region has marked in yellow color). (c) Chemical structures of PTB7-Th, IEICO-4F, and $PC_{71}BM$ molecules.

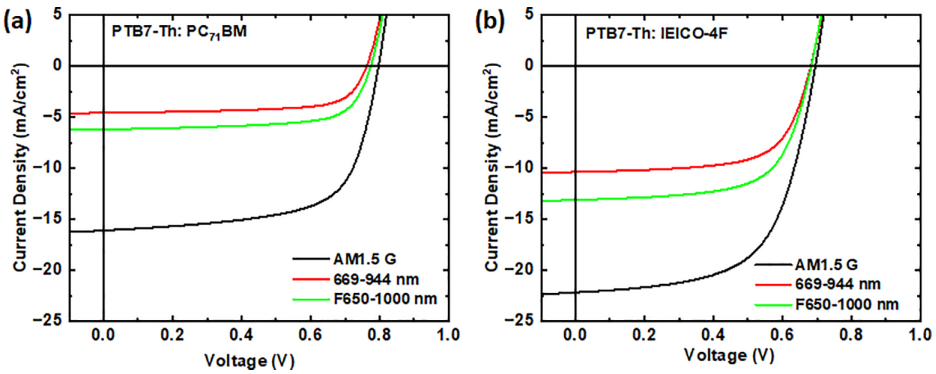

FIG. 2. J-V characteristics of the (a) PTB7-Th: $PC_{71}BM$ device and (b) PTB7-Th: IEICO-4F device under (1 sun) AM1.5G, F650-1000 nm, and 669–945 nm illuminations.

TABLE I. Summary of performance of PTB7-Th: $PC_{71}BM$ and PTB7-Th: IEICO-4F devices measured under 1 sun AM1.5G, F650-1000 nm, and 669–944 nm illumination.

Device	Illumination	V_{oc} (V)	J_{sc} (mA/cm^2)	FF	PCE (A) %	PCE (B) %	Power density (μW/cm^2)
PTB7-Th: $PC_{71}BM$	AM 1.5 G	0.80	16.21	0.66	8.54	—	
	F650-1000 nm	0.77	6.19	0.69	3.31	8.11	3310
	669–944 nm	0.76	4.58	0.69	2.42	6.77	
PTB7-Th: IEICO-4F	AM 1.5 G	0.70	21.91	0.60	9.35	—	
	F650-1000 nm	0.68	13.11	0.65	5.84	14.30	5840
	669–944 nm	0.68	10.38	0.66	4.68	13.10	

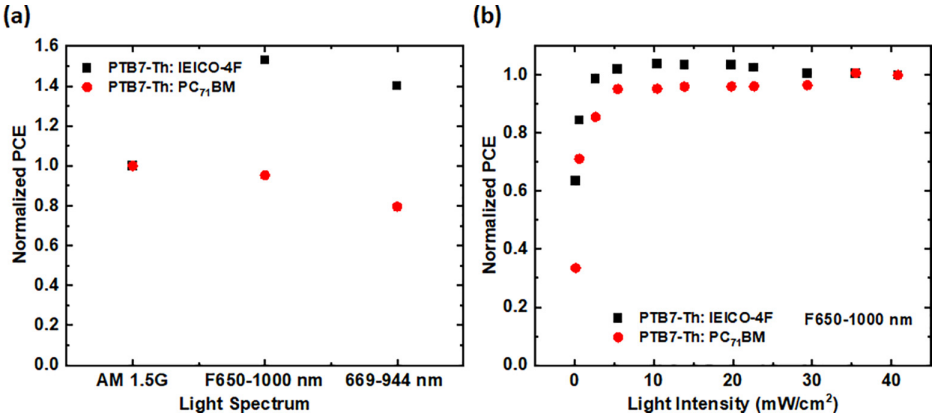

FIG. 3. (a) Normalized PCE (B) of PTB7-Th: $PC_{71}BM$ and PTB7-Th: IEICO-4F devices measured under F650-1000 nm and 669–944 nm incident spectrum, respectively. Data are normalized to their PCE values under 1 sun AM 1.5G illumination (without optical filters). (b) Normalized PCE of PTB7-Th: $PC_{71}BM$ and PTB7-Th: IEICO-4F devices measured under F650-1000 nm as a function of the light intensity. Data are normalized to the PCE at the highest intensity value.

The EQE spectra of the PTB7-Th: $PC_{71}BM$ and PTB7-Th: IEICO-4F devices matches well with the (normalized) absorption spectra of their corresponding films (Fig. S3), which correlates well with the strong absorption of NIR photons by IEICO-4F. The calculated values of the current density (J_{EQE}) from EQE were also well matched with J_{sc} measured from the J–V curves (Table S1). Under the F650–1000 nm illumination, the maximum PCE (A) values of the PTB7-Th: $PC_{71}BM$ and PTB7-Th: IEICO-4F devices were 3.31% and 5.84%, respectively. Similarly, under the 669–944 nm region, these devices delivered PCE (A) of 2.42% and 4.65%, respectively. The J_{sc} was the main parameter that contributed to deliver the higher performance of PTB7-Th: IEICO-4F devices compared to PTB7-Th: $PC_{71}BM$ under the implant illumination region, as IEICO-4F covered the absorption up to NIR wavelengths. It becomes even clearer when PCE(B) was used. For PTB7-Th: IEICO-4F, the PCE (B) was 14.30%, and 13.10% under the F650–1000 nm and 669–944 nm spectrum, respectively. While for PTB7-Th: $PC_{71}BM$ devices, the PCE (B) was 8.11%, and 6.77% under F650–1000 nm and 669–945 nm spectrum, respectively. The PCE (B) of the devices calculated under F650–1000 nm (14.30%) and 669–945 nm (13.10%) spectrum region were higher for the PTB7-Th: IEICO-4F device than its 1 sun AM1.5 G performance [9.35% (without optical filters)]. On the contrary, for the PTB7-Th: $PC_{71}BM$ device, the PCE (B) was low (8.11% and 6.77%) compared to the 1 sun AM1.5G performance (8.54%). The PTB7-Th: IEICO-4F device delivered significantly higher PCE (B) than the PTB7-Th: $PC_{71}BM$ device for potential implant application. The normalized PCE (normalized to their PCE at 1 sun AM1.5G) of $PC_{71}BM$-based and IEICO-4F-based devices under F650–1000 nm and 669–944 nm spectrum is shown in Fig. 3(a). A detailed summary of device performance is shown in Table I.

The light intensity dependent photovoltaic performance was also performed by using neutral density filters. This study aims to compare the OPV devices performance by reducing the incident light intensity at the F650–1000 nm wavelength region to mimics light absorption losses by human skin. Considering that the actual absorption losses could be more complicated, we studied the performance of the OPV devices under a wide range of light intensities relevant to the light absorption loss after passing through skins. There was slightly more reduction in V_{oc} of the $PC_{71}BM$-based device than that of the IEICO-4F-based device with decreasing light intensity [Fig. S4(a)], though the difference is more obvious at lower light intensity. Furthermore, there was an increase in the FF [Fig. S4(b)] of the IEICO-4F-based device down to 5 mW/cm^2 light intensity, while the FF of the $PC_{71}BM$-based device is similar down to 5 mW/cm^2 light intensity. Interestingly, the overall PCE of the IEICO-4F-based device was improved slightly down to 5 mW/cm^2 light intensity under F650–1000 nm illumination [Fig. 3(b)]. On the other hand, the PCE of the $PC_{71}BM$ -based device decrease with lower light intensity, particularly below 5 mW/cm^2 light intensity. The power output generated by IEICO-4F-based OPV is 5840 μW/cm^2 (without the ND filters) under the F650–1000 illumination. Table II summarizes the OPV performances of our devices compared with those reported in the literature for potential implant applications. It shows that our devices have orders of magnitude better PCE and output power density. After considering ~80% performance losses underneath human skin,[8] the OPV could generate enough power (175.2 μW with 0.15 cm^2 device area) to charge batteries to power implant devices.[14]

TABLE II. Summary of performance of the OPV devices in this study and those OPV devices reported for potential implant applications.

Illumination Wavelength(s)	Illumination power	Active layer	V_{oc} (V)	J_{sc} (mA/cm^2)	FF	PCE (%)	Output power density (μW/cm^2)	Ref.
NIR light LED (peak at 780 nm)	210 mW	P3HT: PCBM	0.49	0.7	0.38	—	1303.4	27
		β-carotene/PTCDI-C8	0.11	5.4×10^{-4}	0.18	—	0.1	
980 nm laser	16.9 mW	P3HT: PCBM	0.43	0.058	0.70	0.0124	17.5	28
650–1000 nm	6.09 mW	PTB7-Th: $PC_{71}BM$	0.77	6.19	0.69	8.11	3310	This work
		PTB7-Th: IEICO-4F	0.68	13.11	0.65	14.33	5840	

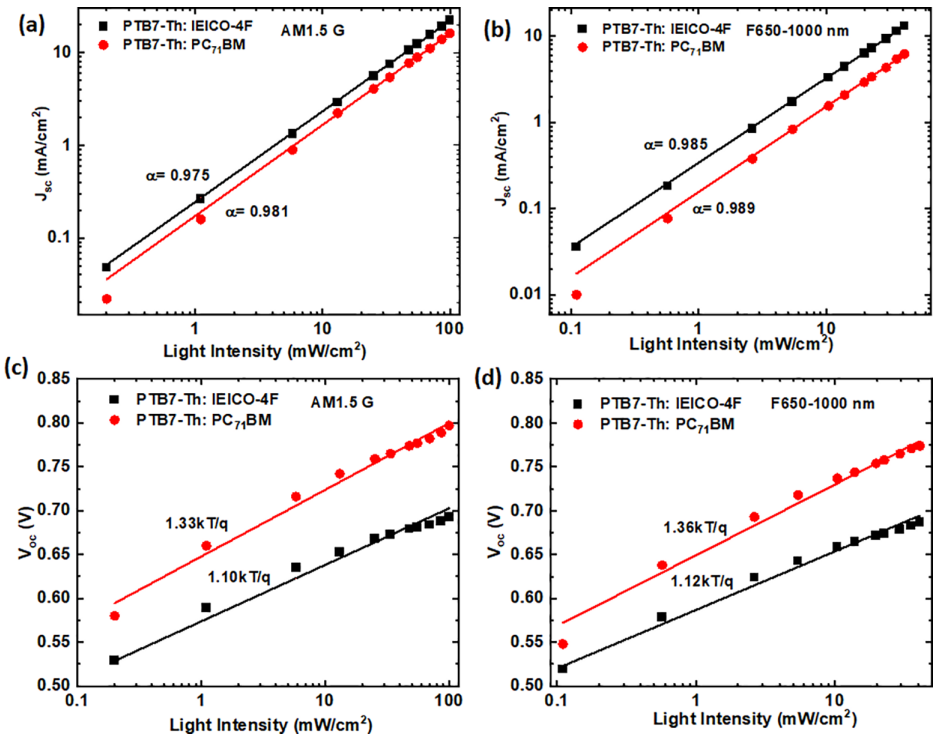

FIG. 4. J_{sc} vs light intensity plots under (a) AM1.5G and (b) F650-1000 incident light spectrum. V_{oc} vs light intensity plots under (c) AM1.5G and (d) F650-1000 incident light spectrum.

Finally, the J–V characteristics under different light intensities were studied in more detail to gain some insight into the charge recombination in the OPV devices under AM 1.5G and F650–1000 nm incident light. It is suggested that $J_{sc} \propto P_{light}^{\alpha}$, where J_{sc}, P_{light}, and α are the short circuit current density, incident light intensity, and charge recombination parameter, respectively.[37] A less than unity value of α indicates bimolecular charge recombination, which can limit performance of the OPV device.[38] As shown in Fig. 4(a), the α values calculated for PTB7-Th: IEICO-4F and PTB7-Th: $PC_{71}BM$ under the AM1.5 G spectrum are 0.975 and 0.981, respectively. The α values under F650–1000 nm illumination are similar to that under AM1.5G illumination with values of 0.985 and 0.989 for PTB7-Th: IEICO-4F and PTB7-Th: $PC_{71}BM$ devices, respectively [Fig. 4(b)]. In addition, the plot of V_{oc} vs P_{light} could provide information about trap-assisted recombination.[39] The data are fitted by following the formula $V_{oc} \propto nkT/q \ln P_{light}$, where n, k, T, and q represent the ideality factor, Boltzmann's constant, absolute temperature, and elementary charge, respectively.[37] As shown in Fig. 4(c), slopes of 1.33kT/q and 1.10kT/q under AM 1.5 G are calculated for PTB7-Th: $PC_{71}BM$ and PTB7-Th: IEICO-4F devices, respectively. The slopes under F650–1000 nm incident light are also similar to that under AM1.5G illumination with the calculated values of 1.36kT/q and 1.12kT/q for PTB7-Th: $PC_{71}BM$ and PTB7-Th: IEICO-4F devices, respectively [Fig. 4(d)]. Therefore, there is no considerable change in the V_{oc} and J_{sc} light dependence between the NIR and AM1.5G (full light spectrum illumination), which implies that there is no adverse effect on the charge recombination under NIR illumination.

In conclusion, we compared the performance of a non-fullerene acceptor-based OPV device (PTB7-Th: IEICO-4F) to a fullerene derivative acceptor-based OPV device (PTB7-Th: $PC_{71}BM$) under 650–1000 nm light illumination as well as under a wide range of light intensity (to mimic the implant light environment). Two methods were used to mimic the light spectrum passing through skin. The first method was by using optical filters, and the second method was by tuning the spectrum of an LED solar simulator. Under 1 sun AM1.5G, the PTB7-Th: $PC_{71}BM$ and PTB7-Th: IEICO-4F OPV devices delivered the PCE of 8.54% and 9.35%, respectively. Interestingly, the PCE of the PTB7-Th: $PC_{71}BM$ and PTB7-Th: IEICO-4F devices under the F650–1000 nm spectrum region were 8.11% and 14.30%, respectively. The high absorption of the IEICO-4F acceptor in the NIR region is the main factor that improves the PCE compared to the $PC_{71}BM$-based device. Importantly, the PCE and power density of the PTB7-Th: IEICO-4F devices are significantly better than previously reported (fullerene derivative-based) OPV devices. As the bandgap of NFA can be tuned easily to absorb at the NIR region, they are an attractive choice for IPV devices. This work demonstrates the prospect of OPVs, especially NFA-based devices, for potential implant applications. However, more research is required in the future for substrate selection, as a flexible substrate could be more practical. Furthermore, research on material biocompatibility, stability, *in vitro* testing under skins, and, ultimately, *in vivo* testing of the devices with the implanted electronic devices is needed.

See the supplementary material for the device structure, LED lights spectrum, supporting EQE, and absorption data.

We are very grateful to the SPECIFIC Innovation and Knowledge Center (No. EP/N020863/1), EPSRC ICASE (No. EP/

S513714/1), and the Welsh European Funding Office (SPARC II) grants for providing financial support.

AUTHOR DECLARATIONS

Conflict of Interest

The authors have no conflicts to disclose.

Author Contributions

Ram Datt: Conceptualization (lead); Data curation (lead); Formal analysis (lead); Writing – original draft (lead); Writing – review and editing (lead). **Harrison Ka Hin Lee**: Conceptualization (equal); Data curation (equal); Formal analysis (equal). **Michael Spence:** Data curation (supporting); Formal analysis (supporting). **Matthew Carnie:** Funding acquisition (equal); Resources (equal); Supervision (equal); Validation (equal); Visualization (equal). **Wing Chung Tsoi**: Conceptualization (equal), Funding acquisition (lead); Investigation (equal); Methodology (equal); Project administration (lead); Resources (equal); Supervision (lead); Validation (equal); Visualization (equal).

DATA AVAILABILITY

The data that support the findings of this study are available within the article and its supplementary material.

REFERENCES

[1]J. Li and X. Wang, Acc. Mater. Res. **2**, 739 (2021).
[2]L. M. Wangatia, S. Yang, F. Zabihi, M. Zhu, and S. Ramakrishna, Curr. Opin. Biomed. Eng. **13**, 25 (2020).
[3]S. Yang, V. Sencadas, S. S. You, N. Z. Jia, S. S. Srinivasan, H. Huang, A. E. Ahmed, J. Y. Liang, and G. Traverso, Adv. Funct. Mater. **31**, 2009289 (2021).
[4]J. Zhao, R. Ghannam, K. O. Htet, Y. Liu, M. Law, V. A. L. Roy, B. Michel, M. A. Imran, and H. Heidari, Adv. Healthc. Mater. **9**, 2000779 (2020).
[5]D. C. Bock, A. C. Marschilok, K. J. Takeuchi, and E. S. Takeuchi, Electrochim. Acta **84**, 155 (2012).
[6]G.-T. Hwang, M. Byun, C. K. Jeong, and K. J. Lee, Adv. Healthc. Mater. **4**, 646 (2015).
[7]D. Barolet, Semin. Cutan. Med. Surg. **27**, 227 (2008).
[8]K. Song, J. H. Han, H. C. Yang, K. I. Nam, and J. Lee, Biosens. Bioelectron. **92**, 364 (2017).
[9]K. Song, J. H. Han, T. Lim, N. Kim, S. Shin, J. Kim, H. Choo, S. Jeong, Y.-C. Kim, Z. L. Wang, and J. Lee, Adv. Healthc. Mater. **5**, 1572 (2016).
[10]A. Haeberlin, A. Zurbuchen, J. Schaerer, J. Wagner, S. Walpen, C. Huber, H. Haeberlin, J. Fuhrer, and R. Vogel, Europace **16**, 1534 (2014).
[11]R. W. Miles, G. Zoppi, and I. Forbes, Mater. Today **10**, 20 (2007).
[12]Y. J. Hung, M. S. Cai, J. F. Chen, H. W. Su, P. C. Jen, P. Chen, C. C. Shih, and T. C. Chang, IEEE J. Photovolt. **8**, 342 (2018).
[13]S. I. Park, G. Shin, A. Banks, J. G. McCall, E. R. Siuda, M. J. Schmidt, H. U. Chung, K. N. Noh, J. G.-H. Mun, J. Rhodes, M. R. Bruchas, and J. A. Rogers, J. Neural Eng. **12**, 056002 (2015).
[14]L. Zhang, Q. Tian, W. Xu, X. Kuang, J. Hu, M. Zhu, J. Liu, and Z. Chen, J. Mater. Chem. **22**, 18156 (2012).
[15]Z. Chen, L. Zhang, Y. Sun, J. Hu, and D. Wang, Adv. Funct. Mater. **19**, 3815 (2009).
[16]H. K. H. Lee, Z. Li, J. R. Durrant, and W. C. Tsoi, Appl. Phys. Lett. **108**, 253301 (2016).
[17]X. Hou, Y. Wang, H. K. H. Lee, R. Datt, N. Uslar Miano, D. Yan, M. Li, F. Zhu, B. Hou, W. C. Tsoi, and Z. Li, J. Mater. Chem. A: Mater. **8**, 21503 (2020).
[18]R. Meitzner, U. S. Schubert, and H. Hoppe, Adv. Energy Mater. **11**, 2002551 (2021).
[19]B. Lee, L. Lahann, Y. Li, and S. R. Forrest, Sustain Energy Fuels **4**, 5765 (2020).
[20]H. K. H. Lee, K. Stewart, D. Hughes, J. Barbé, A. Pockett, R. C. Kilbride, K. C. Heasman, Z. Wei, T. M. Watson, M. J. Carnie, J.-S. Kim, and W. C. Tsoi, Sol. RRL **6**, 2101037 (2022).
[21]Z. Zheng, J. Wang, P. Bi, J. Ren, Y. Wang, Y. Yang, X. Liu, S. Zhang, and J. Hou, Joule **6**, 171 (2022).
[22]B. Kan, F. Ershad, Z. Rao, and C. Yu, Nano Res. **14**, 2891 (2021).
[23]M. J. I. Airaghi Leccardi, N. A. L. Chenais, L. Ferlauto, M. Kawecki, E. G. Zollinger, and D. Ghezzi, Commun. Mater. **1**, 21 (2020).
[24]M. Bolognesi, M. Prosa, and M. Seri, in *Sustainable Strategies in Organic Electronics* (Elsevier, 2022), pp. 297–338.
[25]C. C. Cooksey and D. W. Allen, in *Active and Passive Signatures IV*, edited by G. C. Gilbreath and C. T. Hawley (SPIE, 2013), p. 87340N.
[26]S. L. Jacques, Phys. Med. Biol. **58**, 5007 (2013).
[27]Y.-S. Hsiao, Y.-H. Liao, H.-L. Chen, P. Chen, and F.-C. Chen, ACS Appl. Mater. Interfaces **8**, 9275 (2016).
[28]J.-L. Wu, F.-C. Chen, M.-K. Chuang, and K.-S. Tan, Energy Environ. Sci. **4**, 3374 (2011).
[29]C. W. Tang, Appl. Phys. Lett. **48**, 183 (1986).
[30]G. Li, C.-W. Chu, V. Shrotriya, J. Huang, and Y. Yang, Appl. Phys. Lett. **88**, 253503 (2006).
[31]D. Luo, W. Jang, D. D. Babu, M. S. Kim, D. H. Wang, and A. K. K. Kyaw, J. Mater. Chem. A. Mater. **10**, 3255 (2022).
[32]E. M. Speller, A. J. Clarke, J. Luke, H. K. H. Lee, J. R. Durrant, N. Li, T. Wang, H. C. Wong, J.-S. Kim, W. C. Tsoi, and Z. Li, J. Mater. Chem. A. Mater. **7**, 23361 (2019).
[33]X. Zhan and S. R. Marder, Mater. Chem. Front. **3**, 180 (2019).
[34]T. Kim, J. Choi, H. J. Kim, W. Lee, and B. J. Kim, Macromolecules **50**, 6861 (2017).
[35]Y. Lin and X. Zhan, Mater Horiz **1**, 470 (2014).
[36]R. Datt, Suman, A. Bagui, A. Siddiqui, R. Sharma, V. Gupta, S. Yoo, S. Kumar, and S. P. Singh, Sci. Rep. **9**, 8529 (2019).
[37]X. Hu, R. Datt, Q. He, P. Kafourou, H. K. H. Lee, A. J. P. White, W. C. Tsoi, and M. Heeney, J. Mater. Chem. C. Mater. **10**, 9249 (2022).
[38]X. Song, N. Gasparini, L. Ye, H. Yao, J. Hou, H. Ade, and D. Baran, ACS Energy Lett. **3**, 669 (2018).
[39]N. Gasparini, S. H. K. Paleti, J. Bertrandie, G. Cai, G. Zhang, A. Wadsworth, X. Lu, H.-L. Yip, I. McCulloch, and D. Baran, ACS Energy Lett. **5**, 1371 (2020).